Supporting Information

Reorientational Dynamics of Amyloid-beta from NMR Spin Relaxation and Molecular Simulation

Nasrollah Rezaei-Ghaleh[†,‡,*], *Giacomo Parigi*[§], *Markus Zweckstetter*[†,‡,¥]

[†]Dept. of Neurology, University Medical Center Goettingen, Goettingen, Germany

[‡]Dept. for NMR-based Structural Biology, Max Planck Institute for Biophysical Chemistry, Goettingen, Germany

[§]Magnetic Resonance Center (CERM) and Department of Chemistry "Ugo Schiff", University of Florence, via Sacconi 6, 50121 Sesto Fiorentino, Italy

[¥]Research group for Structural Biology in Dementia, German Center for Neurodegenerative Diseases (DZNE) Goettingen, Goettingen, Germany

Table of Contents

1. Experimental details

Materials

Recombinant ^{15}N-labelled Aβ40 was purchased from rPeptide (Athens, GA). The peptide was solubilized in 20 mM NaOH at a concentration of 2 mg/mL to remove any preformed aggregates and stored at -80 °C until use.

Experimental ^{15}N relaxation rates

^{15}N spin relaxation rates of Aβ40 were measured at three proton Larmor frequencies of 400.13, 600.25 and 701.15 MHz using Bruker (Karlsruhe, Germany) spectrometers equipped with room temperature and cryogenic probes. The NMR sample contained 100 μM uniformly ^{15}N-labelled Aβ40, buffered with 20 mM sodium phosphate (pH 7.4), and 10% D_2O for frequency locking. To minimize protein aggregation, NMR relaxation experiments were performed at 278 K.

^{15}N R_1 rates were measured using conventional pulse sequence schemes with eight relaxation delays spaced between 10 and 800 ms. A train of selective 180 degree ^{1}H pulses during the relaxation block was used to eliminate cross-correlated relaxation effects while minimally perturbing water magnetization [1]. ^{15}N R_2 rates were measured through a CPMG-based pulse sequence with τ_{cp} of 1 ms (ν_{CPMG} = 1000 Hz) and ten relaxation delays spaced between 4 and 240 ms [1]. Residue-specific R_1 and R_2 rates were determined through fitting to single exponential decay functions. The corresponding errors were estimated via 100 Monte Carlo (MC) simulation runs, for which the fit residuals served as random noise. ^{1}H,^{15}N heteronuclear NOEs were obtained by comparison of peak intensities between saturated and reference spectra, using a saturation block of 7.5 s and a total recycle delay of 8 s. Because of the inherently low sensitivity, the heteronuclear NOE experiment was not measured at the 400.13 MHz spectrometer with a room-temperature probe. The exchange-free R_2 rates, R_2^0, were estimated from previously-reported *CCR* rates [2], where the value of κ was evaluated with the magnitude (Δσ) and angle (θ) of the ^{15}N CSA tensor set to -170 ppm and 22.5°, respectively[3]. Data were processed using NMRPipe [4] and analyzed using Sparky 3 (T.D. Goddard and D.G. Kneller, http://www.cgl.ucsf.edu/home/sparky).

2. Spectral density analysis

Reduced spectral density mapping of ^{15}N relaxation rates [5] was achieved using an in-house MATLAB script. Briefly, the ^{15}N relaxation rates R_1 and R_2 and heteronuclear NOE measured at each magnetic field (i.e. 600 and 700 MHz proton Larmor frequency) were converted to three spectral density values, $J(0)$, $J(\omega_N)$ and $J(<\omega_H>)$, where $J(<\omega_H>)$ represents the average between $J(\omega_H+\omega_N)$, $J(\omega_H)$ and $J(\omega_H-\omega_N)$. As a result, the spectral density function was evaluated at five different frequencies: 0, 60, 70, and (effective) 600 and 700 MHz.

3. MD simulation

The MD trajectory was taken from [6]. As described there: the MD simulation of Aβ40 was performed using the a99SB-*disp* force field with the optimized TIP4P-D water model. The simulation started from an extended conformation of Aβ40, solvated in a 60 × 60 × 60 $Å^3$ box containing 6661 water molecules and 50 mM NaCl. The system was initially equilibrated at 300 K and 1 bar for 1 ns, then 30,000-ns production run at 300 K and 1 bar was performed in the NPT ensemble with the Anton specialized hardware at 2.5 fs time step. Nonbonded interactions were truncated at 12 Å and the Gaussian split Ewald method with a 32 × 32 × 32 mesh was used for the electrostatic interactions. The MD frames were saved at 1 ns intervals.

4. MD-based analysis of ^{15}N relaxation rates

Second-order angular autocorrelation functions (ACFs) for the 39 individual backbone N-H vectors of Aβ40 (all residues except D1) were calculated from the MD trajectory. A Gaussian window function with a correlation time of 50 ns was applied to all ACFs to ensure their decay to zero without considerably affecting the initial part of the ACFs. The ACFs were then fitted to exponential decay functions,

$$C(t) = \sum_i S_i^2 \exp(-\frac{t}{\tau_i}) \qquad \text{(S1)}$$

with i=1,2,3, S^2 and τ represent the squared order parameters and correlation times, respectively, and $\sum_i S_i^2 = 1$. Using the best-fit parameters obtained with a three-exponential decay function, which was generally better than one or two-exponential functions, the individual spectral density functions at angular frequency ω were then calculated as:

$$J(\omega) = \frac{2}{5}\ (S_{slow}^2 \frac{\tau_{slow}}{1+ (\omega.\tau_{slow})^2} + S_{int}^2 \frac{\tau_{int}}{1+ (\omega.\tau_{int})^2} + S_{fast}^2 \frac{\tau_{fast}}{1+ (\omega.\tau_{fast})^2}) \qquad \text{(S2)}$$

Finally, ^{15}N longitudinal (R_1) and transverse (R_2) auto-relaxation rates, ^{15}N-^{1}H cross-relaxation rates (σ) and heteronuclear NOEs, and transverse cross-correlated relaxation rates (*CCR*, η_{xy}) were calculated as:

$$R_1 = \left(\frac{d^2}{4}\right)[J(\omega_H - \omega_N) + 3J(\omega_N) + 6J(\omega_H + \omega_N)] + c^2 J(\omega_N) \qquad \text{(S3a)}$$

$$R_2 = \left(\frac{d^2}{8}\right)[4J(0) + J(\omega_H - \omega_N) + 3J(\omega_N) + 6J(\omega_H) + 6J(\omega_H + \omega_N)] + \left(\frac{c^2}{6}\right)[4J(0) + 3J(\omega_N)] \qquad \text{(S3b)}$$

$$\sigma = \left(\frac{d^2}{4}\right)[-J(\omega_H - \omega_N) + 6J(\omega_H + \omega_N)] \qquad \text{(S3c)}$$

$$hetNOE = 1 + \frac{\sigma.\omega_H}{R_1.\omega_N} \qquad \text{(S3d)}$$

$$\eta_{xy} = \frac{\sqrt{3}}{6} c d P_2(cos\theta)[4J(0) + 3J(\omega_N)] \quad \text{(S3e)}$$

where $d = -\frac{\mu_0 \hbar \gamma_H \gamma_N}{4\pi r_{NH}^3}$ and $c = \frac{\gamma_N \Delta\sigma\, B_0}{\sqrt{3}}$. The effective NH bond length of 1.04 Å was used to account for zero-point vibrations [7]. The ^{15}N CSA tensor magnitude ($\Delta\sigma$) was set to -170 ppm. The angle θ between NH bond vectors and the main axis of the ^{15}N CSA tensors was set to 22.5° [3].

5. MD-based analysis of segmental reorientations

Second-order angular ACFs were calculated for the C^A_{i-1},C^A_i and C^A_{i-n},C^A_{i+n} vectors of Aβ40 from the MD trajectory with n=1,2,3,4,5 and 7. The obtained ACFs showed better fits to a three-exponential decay functions when compared to one- and two-exponentials (p-value <0.0001). Using the best-fit parameters obtained with a three-exponential decay function, the weighted-average reorientational correlation times were calculated for the segments of various lengths (as shown in Fig. 2b, inset), with the uncertainties in the correlation times estimated on the basis of fitting errors.

6. MD-based analysis of intramolecular diffusion rates

To compare with the previously reported experimental sm-nsFCS data, where the N- and C-termini of Aβ40 were labelled with Alexa488 and Alexa 647,[8] the end-to-end distance between the N-terminal nitrogen atom of Asp1 and the C-terminal oxygen atom of Val40 was evaluated along the MD trajectory. The end-to-end distance ACF was then calculated. After applying a Gaussian window function with a correlation time of 400 ns to ensure the decay of ACF to zero at very long times without significantly affecting its initial part, the distance ACF was fitted to one- or two-exponential decay functions and the reconfiguration time of the Aβ40 chain between its two termini was determined. The MD-based reconfiguration time required a scaling factor of 0.75±0.05 to match the experimental value. Assuming that the relative motion of the two termini of Aβ40 is best described as diffusion of a Gaussian chain in a square-well potential, the effective end-to-end diffusion coefficient (D) of Aβ40 was estimated through[9]:

$$D = \frac{<r^2>}{6\tau_r} \quad \text{(S4)}$$

where $<r^2>$ is the mean square end-to-end distance from the MD trajectory and τ_r is the MD-based reconfiguration time after scaling by 0.75 (see above). A similar procedure was followed for the analysis of intramolecular diffusion between Tyr10 and Val40.

7. HYCUD calculations

An ensemble of 5000 random Aβ40 structures was generated using the program Flexible-Meccano[10], thereafter side-chain atoms were added by the program SSCOMP. HYCUD calculations were performed as described in [11-12]. Briefly, each member of the Aβ40 ensemble was split into three non-overlapping fragments (residues 1-13, 14-27, 28-40), and hydrodynamic calculation for the isolated fragments were made at 5 °C using the atomic effective radius (AER) of 2.9 Å [13]. The use of this AER value was validated by the comparison between the HYCUD-predicted translational diffusion coefficient and its corresponding hydrodynamic radius (R_h) with the experimental values. After correction for the hydrodynamic drag caused by nearby fragments, the ensemble-average rotational correlation time of each fragment was obtained. The uncertainty of the HYCUD-predicted correlation time was estimated from the standard deviation of the results obtained for 10 sub-ensembles each containing 500 conformers.

8. Supporting Figures

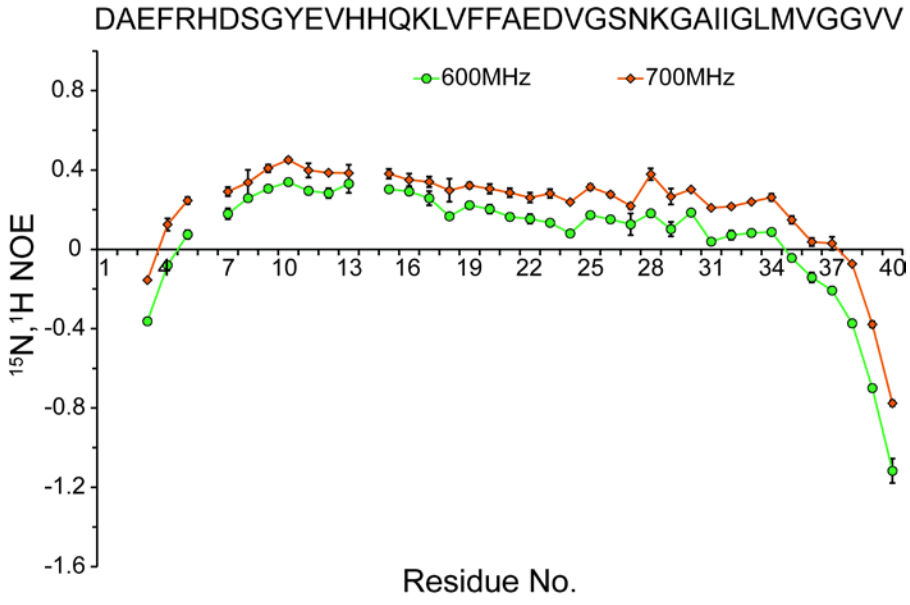

Figure S1. ^{1}H,^{15}N steady-state heteronuclear Overhauser (hetNOE) of Aβ40 at two proton Larmor frequencies of 600 and 700 MHz.

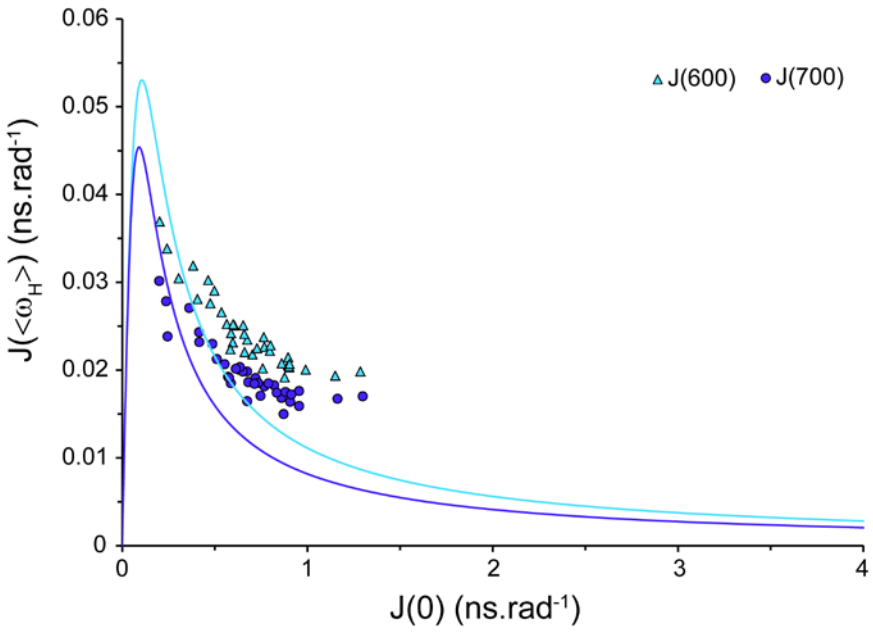

Figure S2. Dependence of spectral densities at effective proton Larmor frequencies, $J(<\omega_H>)$, on the spectral densities at frequency 0, $J(0)$, revealing a clear deviation from a single-Lorentzian profile expected for a rigid-body reorientational motion governed by a single correlation time (solid line). Most residues possess $J(<\omega_H>)$ larger than what would be expected for their $J(0)$ values.

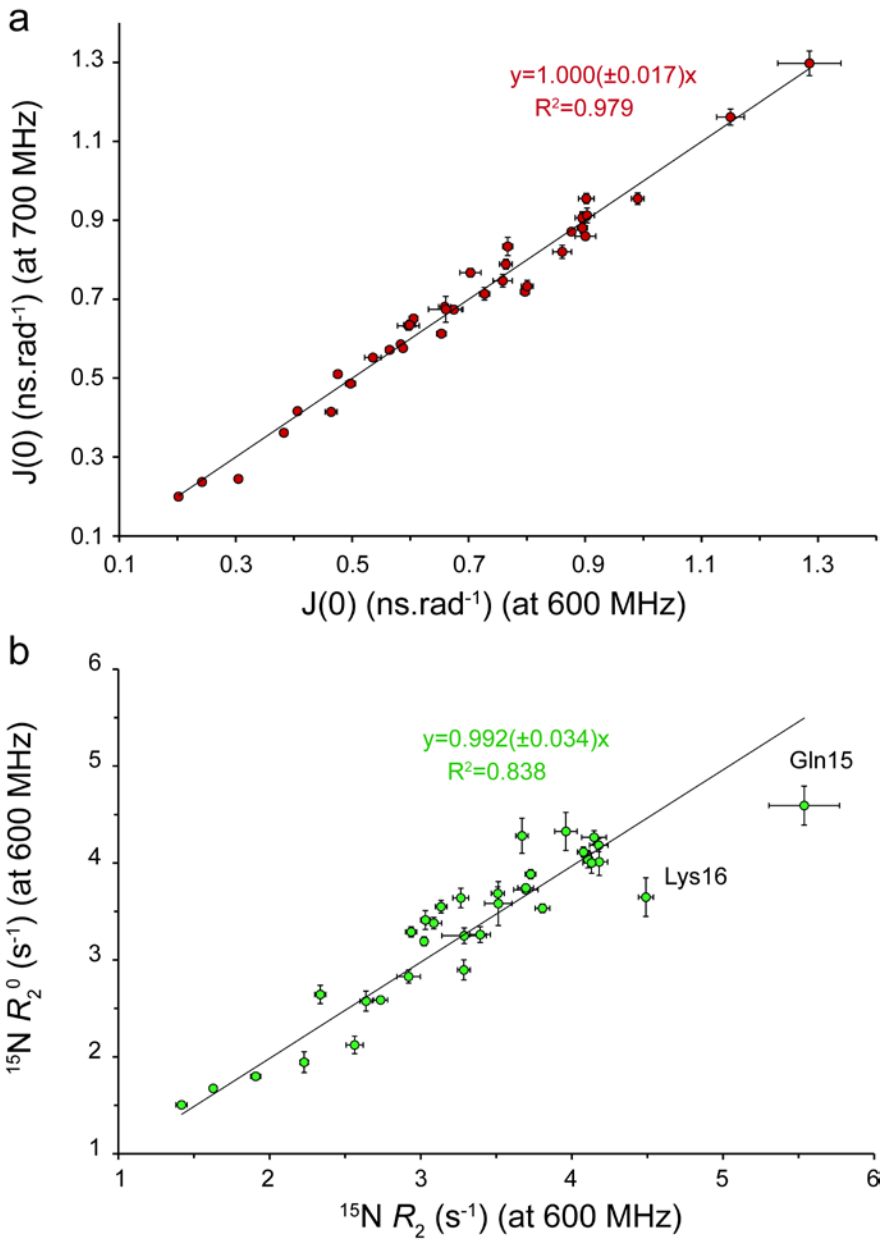

Figure S3. Contribution of conformational exchange to Aβ40 relaxation rates. a) The $J(0)$ values obtained from the spectral density analysis of ^{15}N relaxation rates at two magnetic fields show close agreement, suggesting that the field-dependent exchange-mediated relaxation does not significantly contribute to R_2. b) The exchange-free R_2 rates estimated using *CCR* rates are in close agreement with the R_2 rates measured at 600 MHz, further supporting the negligible contribution of conformational exchange to relaxation rates. The largest deviations were observed for residues Gln15 and Lys16, probably due to the protonation-deprotonation of their nearby Histidines 13 and 14.

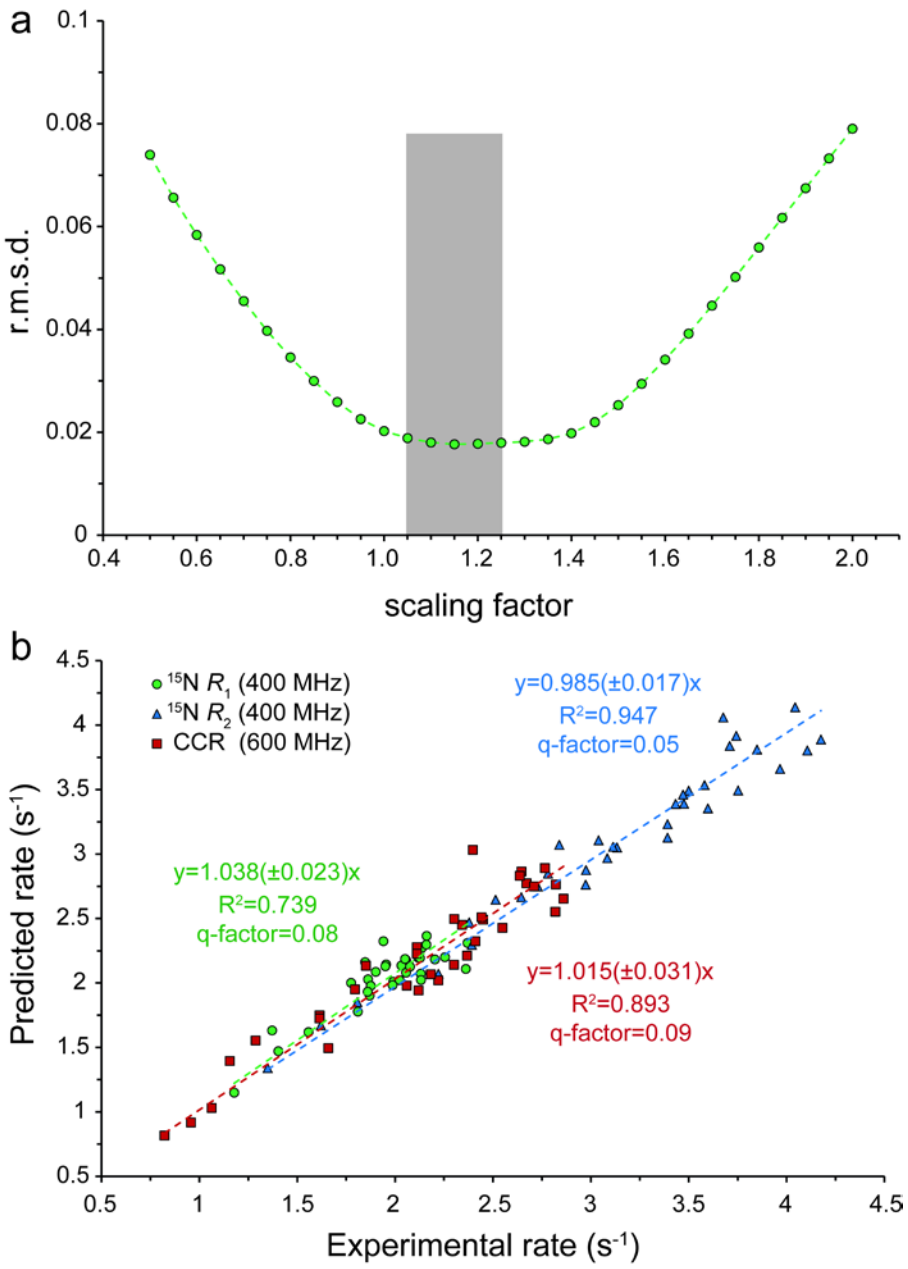

Figure S4. Temporal rescaling of the MD trajectory of Aβ40, on the basis of ^{15}N R_1 and R_2 rates measured at proton Larmor frequencies of 600 and 700 MHz. a) When combined with the order parameter optimization, the best agreement between the MD-predicted and experimental rates were achieved using a scaling factor of 1.15±0.10 for intermediate motions (shaded area). The r.m.s.d was calculated as $rmsd = sqrt[(\left(\frac{R_{1,600,pred}-R_{1,600,exp}}{R_{1,600,exp}}\right))^2 + \left(\frac{R_{2,600,pred}-R_{2,600,exp}}{R_{2,600,exp}}\right))^2 + \left(\frac{R_{1,700,pred}-R_{1,700,exp}}{R_{1,700,exp}}\right))^2 + \left(\frac{R_{2,700,pred}-R_{2,700,exp}}{R_{2,700,exp}}\right))^2/4]$. b) Cross-validation of the optimized order parameters by three experimental rates, ^{15}N R_1 and R_2 rates at proton Larmor frequency of 400 MHz and *CCR* rates at 600 MHz.

9. References

1. Palmer, A. G., 3rd. Nmr probes of molecular dynamics: overview and comparison with other techniques. *Annu. Rev. Biophys. Biomol. Struct.* **2001,** *30*, 129-55.
2. Rezaei-Ghaleh, N.; Giller, K.; Becker, S.; Zweckstetter, M. Effect of zinc binding on beta-amyloid structure and dynamics: implications for Abeta aggregation. *Biophys. J.* **2011,** *101* (5), 1202-11.
3. Kaderavek, P.; Zapletal, V.; Rabatinova, A.; Krasny, L.; Sklenar, V.; Zidek, L. Spectral density mapping protocols for analysis of molecular motions in disordered proteins. *J. Biomol. NMR* **2014,** *58* (3), 193-207.
4. Delaglio, F.; Grzesiek, S.; Vuister, G. W.; Zhu, G.; Pfeifer, J.; Bax, A. NMRPipe: a multidimensional spectral processing system based on UNIX pipes. *J. Biomol. NMR* **1995,** *6* (3), 277-93.
5. Farrow, N. A.; Zhang, O.; Forman-Kay, J. D.; Kay, L. E. Comparison of the backbone dynamics of a folded and an unfolded SH3 domain existing in equilibrium in aqueous buffer. *Biochemistry* **1995,** *34* (3), 868-78.
6. Robustelli, P.; Piana, S.; Shaw, D. E. Developing a molecular dynamics force field for both folded and disordered protein states. *Proc. Natl. Acad. Sci. U. S. A.* **2018,** *115* (21), E4758-E4766.
7. Case, D. A. Calculations of NMR dipolar coupling strengths in model peptides. *J. Biomol. NMR* **1999,** *15* (2), 95-102.
8. Meng, F.; Bellaiche, M. M. J.; Kim, J. Y.; Zerze, G. H.; Best, R. B.; Chung, H. S. Highly Disordered Amyloid-beta Monomer Probed by Single-Molecule FRET and MD Simulation. *Biophys. J.* **2018,** *114* (4), 870-884.
9. Nettels, D.; Gopich, I. V.; Hoffmann, A.; Schuler, B. Ultrafast dynamics of protein collapse from single-molecule photon statistics. *Proc. Natl. Acad. Sci. U. S. A.* **2007,** *104* (8), 2655-60.
10. Ozenne, V.; Bauer, F.; Salmon, L.; Huang, J. R.; Jensen, M. R.; Segard, S.; Bernado, P.; Charavay, C.; Blackledge, M. Flexible-meccano: a tool for the generation of explicit ensemble descriptions of intrinsically disordered proteins and their associated experimental observables. *Bioinformatics* **2012,** *28* (11), 1463-70.
11. Rezaei-Ghaleh, N.; Klama, F.; Munari, F.; Zweckstetter, M. Predicting the rotational tumbling of dynamic multidomain proteins and supramolecular complexes. *Angew. Chem. Int. Ed.* **2013,** *52* (43), 11410-4.
12. Rezaei-Ghaleh, N.; Klama, F.; Munari, F.; Zweckstetter, M. HYCUD: a computational tool for prediction of effective rotational correlation time in flexible proteins. *Bioinformatics* **2015,** *31* (8), 1319-21.
13. Ortega, A.; Amoros, D.; Garcia de la Torre, J. Prediction of hydrodynamic and other solution properties of rigid proteins from atomic- and residue-level models. *Biophys. J.* **2011,** *101* (4), 892-8.